Proceedings of the ASME 2017 Pressure Vessels & Piping Conference
SAND2017-2064C
PVP2017
July 16-20, 2017, Waikoloa, Hawaii, USA

PVP2017-65948

ORIENTATION EFFECTS ON FATIGUE BEHAVIOR OF ADDITIVELY MANUFACTURED STAINLESS STEEL

Thale R. Smith
University of California, Davis
Davis, CA, USA

Joshua D. Sugar
Sandia National Laboratories
Livermore, CA, USA

Chris San Marchi
Sandia National Laboratories
Livermore, CA, USA

Julie M. Schoenung
University of California, Irvine
Irvine, CA, USA

ABSTRACT

Direct energy deposition (DED) is an additive manufacturing process that can produce complex near-net shape metallic components in a single manufacturing step. DED additive manufacturing has the potential to reduce feedstock material waste, streamline manufacturing chains, and enhance design flexibility. A major impediment to broader acceptance of DED technology is limited understanding of defect populations in the novel microstructures produced by DED and their relationship to process parameters and resultant mechanical properties. A design choice as simple as changing the build orientation has been observed to result in differences as great as ~25% in yield strength for type 304L austenitic stainless steel deposited with otherwise identical deposition parameters. To better understand the role of build orientation and resultant defect populations on fatigue behavior in DED 304L, tension-tension fatigue testing has been performed on circumferentially notched cylindrical test specimens extracted from both vertical and horizontal orientations relative to the build direction. Notched fatigue behavior was found to be strongly influenced by the manufacturing defect populations of the material for different build orientations.

INTRODUCTION

Direct energy deposition (DED) additive manufacturing (AM) is an emerging technology capable of producing near-net shape engineering components of high geometric complexity in a single manufacturing step [1]. This is accomplished through the sequential addition of material by laser melting of a feedstock powder fed by an inert gas stream as depicted in Figure 1. Owing to the additive nature of the process and the elimination of fabrication steps in the manufacturing chain, DED offers the potential to both reduce material scrap rates and enhance design flexibility [1, 2]. These benefits have yet to be fully realized by widespread adoption of DED AM in large part due to uncertainty in the final mechanical properties of the as-deposited materials [3].

Austenitic stainless steels produced by DED have been studied extensively, with many studies reporting monotonic mechanical behavior, heterogenous microstructures, and manufacturing defects produced in the materials by the DED process [4-7]. In fully dense materials, this mechanical property variability stems from variability in the microstructures; however, the specific role various microstructural features play in materials performance (e.g., strength, ductility, fracture resistance, fatigue behavior) has yet to be fully delineated [7, 8]. Because the geometry of a component and the properties of the material are produced in a single manufacturing step during DED, it is necessary to develop a better understanding of how local processing conditions influence microstructures and mechanical properties.

Additionally, since the service life of engineering components is often dictated by the mechanical response of materials under cyclic loading conditions, it is also imperative to understand the fatigue behavior of DED austenitic stainless steels. Considerably fewer studies have been performed to assess the fatigue behavior of DED austenitic stainless steels, and the relationship of fatigue behavior to processing conditions has not been rigorously evaluated [9, 10]. Furthermore, to our knowledge, no reports have yet been published on the notched fatigue behavior of DED austenitic stainless steels. Thus, it is the goal of this work to assess the variation in tensile and notched fatigue behavior of DED austenitic stainless steel due to variation in the build geometry orientation.

EXPERIMENTAL PROCEDURES

A single austenitic stainless steel composition (Table 1), conforming to the requirements of a 304L grade alloy, was evaluated in this study [11]. The particle size of the commercial gas atomized powder ranged from 45 to 105 μm. Test specimens were extracted from horizontal (H) and vertical (V) rectilinear builds (Figure 2) measuring approximately 4 cm x 4 cm x 1 cm (tensile) and 6 cm x 4 cm x 1 cm (fatigue). Builds were deposited on 5 mm thick 304L austenitic stainless steel plates in a Laser Engineered Net Shaping 750 workstation utilizing the time-invariant processing parameters in Table 2.

Standard subsized E8 tensile specimens were extracted from the 4 cm x 4 cm x 1 cm deposits with a gauge diameter of 2.87 mm [12]. Specimens were tested under ambient conditions utilizing a constant displacement rate corresponding to a strain rate of approximately 10^{-3} s^{-1}.

For tension-tension fatigue testing, a circumferential notched cylindrical test specimen geometry was used, similar to that described by ASTM G142-98 [13]. The specimens had a reduced section diameter of 5.7 mm, with a minimum diameter of 4.0 mm at the notch root. The notch root radius was 0.083 mm with a notch angle of 60°. This U-shaped notch groove corresponds to an elastic stress concentration factor (Kt) of approximately 4 [14]. Load controlled tests were conducted to failure under ambient conditions at a load-ratio of 0.1 (ratio of minimum to maximum load, R) with a loading frequency of 1 Hz. The maximum stress was calculated from the initial cross-sectional area of the minimum diameter and the maximum applied load. Crack initiation was evaluated using the direct-current potential difference (DCPD) method, utilizing the same spot welded configuration for the current and voltage sensing leads as in previous investigations of similar specimens [15].

Cross sections for metallographic examination were prepared by grinding/polishing with incrementally finer abrasives. Polished samples were then electropolished using a LectroPol-5 (Struers) in an electrolyte of approximately 10% perchloric acid. Electron backscattered diffraction (EBSD) experiments were carried out in a FEI Helios dual beam scanning electron microscope/focused ion beam (SEM)/(FIB). Scan steps ranging from 0.4-1.8 μm were utilized for EBSD mapping depending on the size of the region of interest. Kernal average misorientation (KAM) maps were calculated from the EBSD data using the Channel5 software by applying a 3x3 square filter and an exclusion angle of 5 degrees. Fracture surfaces were evaluated using a Keyence VHX-5000 digital confocal microscope.

RESULTS

Tensile Builds

Archimedes' method density measurements of material from both orientations of the DED 304L tensile builds indicated densities exceeding 99% of the theoretical density for a 304L grade stainless steel [16]. Engineering tensile stress-strain curves for DED 304L are shown in Figure 3, along with previously reported tensile data for forged 304L and 308L/304L weld metal [17, 18]. The H-DED 304L exhibited the highest 0.2% yield strength (S_y) and ultimate strength (S_u) with values of 552 MPa and 730 MPa, respectively. The V-DED 304L exhibited a lower S_y of 440 MPa, but a higher total elongation (El_t) of 70% (compared to 51% for the H-DED 304L). Due to the geometry of the builds, the H-DED specimens were extracted from a bulk material that was much nearer and with a greater relative contact area to the deposition substrate than that from which the V-DED specimens were made. The tensile behavior of the forged 304L was nearly identical to that of the V-DED 304L, while the 308L/304L weld exhibited lower strength and total elongation. The results of the tensile tests are summarized in Table 3. The DED 304L from both orientations exhibited a combination of strength and ductility that exceeds the minimum requirements defined for annealed austenitic stainless steels in standards such as ASTM A479 [11].

EBSD experiments (Figure 4) were performed to characterize the microstructures of the DED, forged, and weld materials. Despite the similarity in tensile properties to the forged 304L, the elongated, columnar grain structure of the DED 304L is qualitatively more similar to that observed in the 308L/304L weld, albeit at a significantly finer length scale. The local misorientations calculated and shown in the KAM maps reveal that all of the materials retain micro-scale strain characteristic of their processing history [19]. The magnitude of the strain is the greatest in the forged material, and both the DED and weld material exhibit heterogeneity in strain distribution at the length scale of the fusion zone.

Fatigue Builds

Archimedes' method density measurements of the V-DED 304L fatigue build revealed density exceeding 99% of the theoretical density for a 304L grade stainless steel, while material from the H-DED 304L was measured to be 97% dense. The tension-tension notched fatigue life test results for the DED 304L are shown in Figure 5. Fatigue data for circumferentially notched specimens of wrought 316L in the annealed (AN) and strain hardened (SH) conditions are included for comparison [20, 21]. For all applied maximum stresses, the test specimens from the horizontal build orientation exhibited diminished fatigue life compared to specimens obtained from the vertical build orientation. Replicate tests of the DED materials were performed at a maximum stress of 305 MPa. The 63% difference in cycles to failure for the duplicate tests of the H-DED 304L compared to the 12% difference of the V-DED duplicate tests further shows a greater variability in the fatigue behavior of the less dense material. A power-law fit of the AN 316L is shown to indicate the trend of fatigue life with applied maximum stress [15]. It can be seen that the trend in notched fatigue life with applied maximum stress is similar between the AN 316L and the V-DED 304L; however, the SH 316L exhibits a slight shift toward longer fatigue life at similar applied maximum stresses.

Figure 6 shows a comparison of fatigue life and crack initiation life for the V-DED 304L notched specimens. At high applied maximum stress, fatigue crack growth represents a

large fraction of the total fatigue life. With decreasing applied maximum stress, fatigue crack growth occurs over a smaller fraction of the total fatigue life, as indicated by the convergence of the extrapolated power-law fit trend lines with increasing load cycles. Such a trend in fatigue crack growth has also been observed in wrought 21Cr-6Ni-9Mn austenitic stainless steels, suggesting analogous fatigue crack growth behavior of fully dense DED and wrought austenitic stainless steels [15].

Post-mortem evaluation of the DED 304L fatigue specimen fracture surfaces was performed to identify defects influencing the fatigue behavior of the materials. The fracture surfaces of the DED fatigue specimens subjected to a maximum stress of~305 MPa are shown in Figure 7. The side-view photographs in the top row show the significant deviation of the fatigue fractures from the plane of the notch root in the short fatigue life H-DED specimens (Figure 7 C,D), compared to the longer fatigue life V-DED specimens (Figure 7 A,B). The confocal micrographs in the middle row further reveal the presence of irregularly shaped defects containing partially melted particles near regions where the fatigue cracks deviated from the notch root plane. The colored height maps show further quantitative evidence that the fatigue crack deflects from the notch root plane in the material with lower density and greater defect population.

DISCUSSION

The mechanical testing and structural characterization results show that the unique characteristics of microscopic defects and gross build defects observed in the type 304L austenitic stainless steel produced by the DED can be linked to the mechanical performance of the materials. For certain deposition conditions, the DED material exhibited monotonic and cyclic mechanical properties consistent with those reported for conventionally fabricated austenitic stainless steels; however, the orientation of the build geometry significantly affected the resulting properties. The implications of the defect populations and orientation dependent mechanical properties are further explored in the following sections.

Microstructure and Tensile Properties

The fusion zone microstructures observed in both the DED 304L and 308L/304L weld suggest that the physical mechanisms driving microstructural development during the two processes are similar. This makes sense given a molten fusion zone is formed in both processes by a locally applied heat source and solidification of the fusion zone occurs as the heat source advances. Additionally, the material experiences a local thermo-mechanical state during processing that has been shown to induce variability in the yield strength of material from multi-pass 308L/304L welds [22, 23]. The yield strength of the first weld pass is significantly greater than the yield strength of the final weld pass. This trend in variability is similar to the significantly greater yield strength of the H-DED material extracted a short distance from the substrate compared to the V-DED material extracted far from the substrate. During DED and welding, thermal expansion of locally heated material is inhibited by the constraints imposed by the surrounding material, such that the material may plastically deform to accommodate the thermal strains. Deposited material undergoes further plastic strain due to subsequent passes of the heat source; however, accounting for this effect is complicated by concurrent annealing of the material [24].

It is believed that the total accumulation of plastic strain results in strain hardening in multi-pass welds, where higher densities of dislocations in the initial weld pass than the final weld pass have been reported [23]. Because such crystallographic defects associated with these strains cause location dependent distortions of the electron diffraction patterns for a given grain orientation, the KAM maps in Figure 4 provide evidence of the presence of process induced strains in both the weld and DED materials [19]. In the case of the DED material, the comparatively higher yield strength of the H-DED build suggests this material experienced greater strain hardening. The relatively larger build footprint of the H-DED build (16 cm^2 vs 4 cm^2) in contact with the substrate may have caused greater strain in the material both due to the greater constraint imposed on the larger area of material deposited on the base plate, as well as due to the presence of steeper thermal gradients as heat is conducted through the large area, short build more efficiently. Despite evidence of significant strain hardening in both weld and DED materials, the comparatively greater magnitude of KAM measured in the forged 304L, which displayed near identical properties to the V-DED 304L, suggests further investigation is required to reveal the extent of the strain hardening effect on the mechanical properties of DED austenitic stainless steels.

Manufacturing Defects and Fatigue Properties

The notched fatigue behavior of the DED material was influenced more strongly by the manufacturing defect population than by the microstructural features present, as shown by the correlation of lower density, diminished fatigue life, and evidence of the significant influence of lack of fusion defects on the fracture morphologies observed in the post-mortem investigation of the H-DED 304L fatigue specimen fracture surfaces. Lack of fusion defects develop due to inadequate penetration of a deposited layer into previously deposited material [25]. Penetration depends on geometry of the molten fusion zone, which in turn is strongly influenced by local thermal conditions [26]. Given that the horizontal fatigue build had the largest contact area of any build with the substrate and the previous discussion suggesting less heat is expected to build up for the large contact area and short horizontal build, it is possible that excessively steep thermal gradients resulted in insufficient deposition penetration. Additionally, there may have been some subtle differences in processing conditions resulting from the different lasers utilized to produce the tensile and fatigue builds.

The fatigue testing results of the dense V-DED 304L illustrates the superior fatigue behavior when manufacturing defects are minimized. Interestingly, even though the fracture surfaces of the higher density V-DED 304L fatigue specimens

displayed some evidence of partially melted particles and lack of fusion defects, the fatigue behavior of the material was found to exhibit similar fatigue life as previously reported for wrought austenitic stainless steels [20, 21]. This suggests that DED 304L can be defect tolerant, consistent with the high intrinsic toughness of austenitic stainless steels. Furthermore, since it was observed that the higher strength SH 316L exhibited improved fatigue properties compared to the AN 316L, it seems that further investigation is necessary to assess the effect of strength on fatigue behavior in fully dense DED austenitic stainless steels.

SUMMARY

This paper represents preliminary progress made in understanding the effect of build orientation on the tensile and notched fatigue behavior of DED austenitic stainless steel. Given the data presented illustrating DED manufacturing defects, microstructures, monotonic tensile behavior, and cyclic tensile behavior, the following conclusions are provided:

- Fully dense DED austenitic stainless steel exhibits cyclic and monotonic tensile behavior commensurate with conventionally manufactured metals.
- Under time-invariant DED processing conditions, build orientation can substantially alter characteristics of both manufacturing defect and microstructural defect populations.
- The significant difference of ~25% in tensile yield strength observed between the horizontal and vertical build geometries is consistent with previous studies on fully dense DED austenitic stainless steel and is likely attributable to microstructural heterogeneity within each build arising from variation of the thermo-mechanical state experienced by the build material due to variations in distance from the substrate.
- Manufacturing defects strongly influence variability in fatigue life and fatigue fracture behavior in DED austenitic stainless steel.

ACKNOWLEDGMENTS

T. R. Smith gratefully acknowledges support from the Sandia National Laboratory Campus Executive Fellowship. Dr. B. Zheng, J. Haley, and K. Wellmon are thanked for valuable technical discussions. A. Gardea is thanked for metallographic preparation assistance. Sandia National Laboratories is a multi-program laboratory managed and operated by Sandia Corporation, a wholly owned subsidiary of Lockheed Martin Corporation, for the U.S. Department of Energy's National Nuclear Security Administration under contract DE-AC04-94AL85000.

REFERENCES

[1] Zheng B, Xiong Y, Nguyen J, Smugeresky JE, Zhou Y, Lavernia EJ, et al. Powder Additive Processing with Laser Engineered Net Shaping. In: Smit LJ, Van Dijk JH, editors. Powder Metallurgy Research Trends: Nova Science Publishers, Inc.; 2009. p. 125-90.

[2] Tammas-Williams S, Todd I. Design for additive manufacturing with site-specific properties in metals and alloys. Scripta Materialia. 2016.

[3] Yadollahi A, Shamsaei N. Additive Manufacturing of Fatigue Resistant Materials: Challenges and Opportunities. International Journal of Fatigue. 2017.

[4] Griffith ML, Ensz MT, Puskar JD, Robino CV, Brooks JA, Philliber JA, et al. Understanding the Microstructure and Properties of Components Fabricated by Laser Engineered Net Shaping (LENS). MRS Online Proceedings Library. 2000;625.

[5] Yu J, Rombouts M, Maes G. Cracking behavior and mechanical properties of austenitic stainless steel parts produced by laser metal deposition. Materials & Design. 2013;45:228-35.

[6] Yadollahi A, Shamsaei N, Thompson SM, Seely D. Effects of process time interval and heat treatment on the mechanical and microstructural properties of direct laser deposited 316L stainless steel. Materials Science and Engineering: A. 2015.

[7] Wang Z, Palmer TA, Beese AM. Effect of processing parameters on microstructure and tensile properties of austenitic stainless steel 304L made by directed energy deposition additive manufacturing. Acta Materialia. 2016;110:226-35.

[8] Zheng B, Zhou Y, Smugeresky JE, Schoenung JM, Lavernia EJ. Thermal behavior and microstructure evolution during laser deposition with laser-engineered net shaping: Part II. Experimental investigation and discussion. Metallurgical and Materials Transactions a-Physical Metallurgy and Materials Science. 2008;39A:2237-45.

[9] Xue Y, Pascu A, Horstemeyer MF, Wang L, Wang PT. Microporosity effects on cyclic plasticity and fatigue of LENS™-processed steel. Acta Materialia. 2010;58:4029-38.

[10] Ganesh P, Kaul R, Sasikala G, Kumar H, Venugopal S, Tiwari P, et al. Fatigue Crack Propagation and Fracture Toughness of Laser Rapid Manufactured Structures of AISI 316L Stainless Steel. Metallogr Microstruct Anal. 2014;3:36-45.

[11] ASTM A479: Standard Specification for Stainless Steel Bars and Shapes for Use in Boilers and Other Pressure Vessels. ASTM International; 2016.

[12] E8 A. Standard test methods for tensile testing of metallic materials. Annual book of ASTM standards. 2015.

[13] ASTM G142: Standard Test Method for Determination of Susceptibility of Metals to Embrittlement in Hydrogen Containing Environments at High Pressure, High Temperature, or Both. ASTM International; 2016.

[14] Pilkey W. Petersons stress concentration factors. 1997.

[15] San Marchi C, Somerday B, Nibur K. Fatigue crack initiation in hydrogen-precharged austenitic stainless steel. : Somerday BP, and Sofronis P, editors, H, Hydrogen-Materials Interactions (Proceedings of the 2012 International Hydrogen Conference, Moran WY, 2012): ASME Press; 2014. p. 365-73.

[16] McGuire MF. Stainless steels for design engineers: Asm International; 2008.

[17] Ronevich JA, San Marchi CW, Balch DK. PVP2017-65603: Temperature effects on fracture thresholds of hydrogen precharged stainless steel welds. ASME Pressure Vessels and Piping Conference. 2017.
[18] Jackson H, San Marchi C, Balch D, Somerday B, Michael J. Effects of Low Temperature on Hydrogen-Assisted Crack Growth in Forged 304L Austenitic Stainless Steel. Metall and Mat Trans A. 2016;47:4334-50.
[19] Wright SI, Nowell MM, Field DP. A Review of Strain Analysis Using Electron Backscatter Diffraction. Microscopy and Microanalysis. 2011;17:316-29.
[20] San Marchi C, Zimmerman JA, Tang X, Kernion SJ, Thürmer K, Nibur KA. Fatigue Life of Austenitic Stainless Steel in Hydrogen Environments. 2015:V06BTA015.
[21] Nibur KA, San Marchi CW. PVP2017-65978: Notched fatigue of austentic alloys in hydrogen. ASME Pressure Vessels and Piping Conference. 2017.
[22] Balch DK, San Marchi C. Effect of Hydrogen on Tensile Strength and Ductility of Multi-Pass 304L/308L Austenitic Stainless Steel Welds. ASME 2015 Pressure Vessels and Piping Conference: American Society of Mechanical Engineers; 2015.
[23] King R, Stiegler J, Goodwin G. Relation between mechanical properties and microstructure in CRE type 308 weldments. Welding journal. 1974;53:307.
[24] Francis J, Bhadeshia H, Withers P. Welding residual stresses in ferritic power plant steels. Materials Science and Technology. 2007;23:1009-20.
[25] Mukherjee T, Zuback J, De A, DebRoy T. Printability of alloys for additive manufacturing. Scientific reports. 2016;6.
[26] Pollard B. The effects of minor elements on the welding characteristics of stainless steel. Welding Journal. 1988;67:202s-13s.

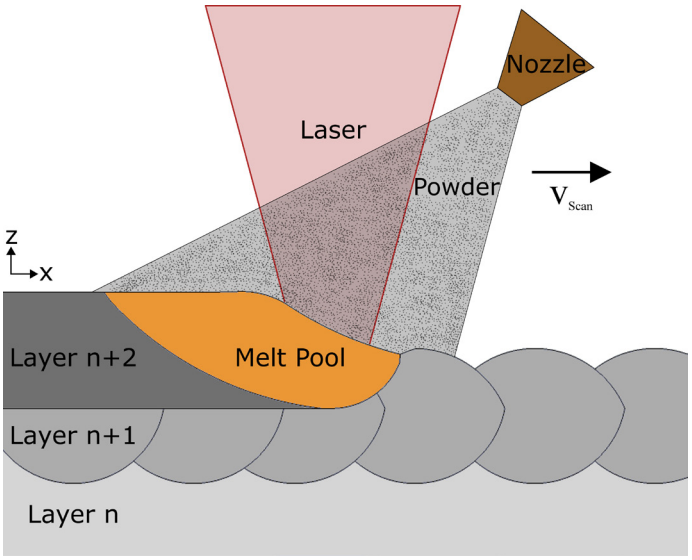

Figure 1. Schematic representation of the direct energy deposition (DED) additive manufacturing process shown in cross-section. The z-axis is parallel to the build direction.

Table 1. Composition (wt%) of the gas atomized (GA) austenitic stainless steel powder used in this study.

Alloy	Fe	Cr	Ni	Mn	Mo	N	C	Si	O	S	P
304L	Bal.	19.4	10.0	1.49	0.03	0.09	0.013	0.54	0.02	0.006	0.008

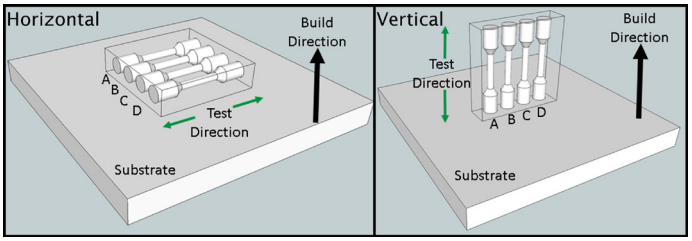

Figure 2. Schematic of the build orientations with respect to the build and extracted specimen loading directions.

Table 2. Deposition parameters utilized during DED of the monotonic and cyclic test specimen builds.

Monotonic			Cyclic		
Deposition Parameter	Value	Unit	Deposition Parameter	Value	Unit
Laser	Nd:Yag	-	Laser	Yb:Fiber	-
Laser Power	400	W	Laser Power	400	W
Scan speed	17	mm/s	Scan speed	11	mm/s
Hatch increment	0.41	mm	Hatch increment	0.46	mm
Layer increment	0.25	mm	Layer increment	0.34	mm
Hatch rotation	90	degrees	Hatch rotation	90	degrees
Powder feed rate	16	g/min	Powder feed rate	34	g/min
Oxygen concentration	<15	ppm	Oxygen concentration	<15	ppm

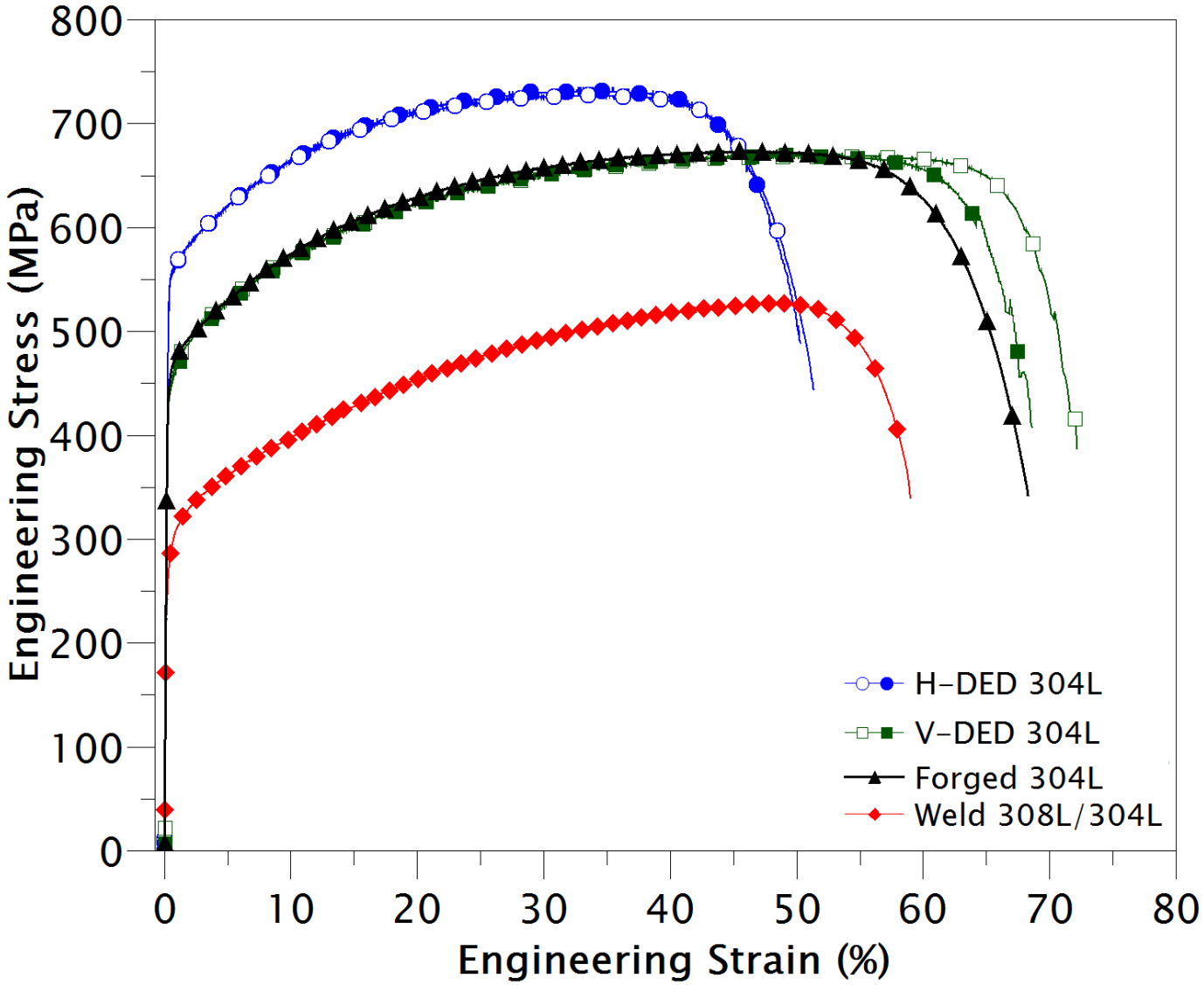

Figure 3. Comparison of monotonic tensile behavior of DED, forged [18], and weld [17] austenitic stainless steels.

Table 3. Tensile properties of DED, weld, and forged austenitic stainless steels.

Alloy	*Processing*	*Sy* (MPa)	*Su* (MPa)	*El$_t$* (%)
304L	H-DED	552	730	51
	V-DED	440	670	70
304L[22]	Forged	452	674	68
308L/304L[21]	Weld	384	596	46

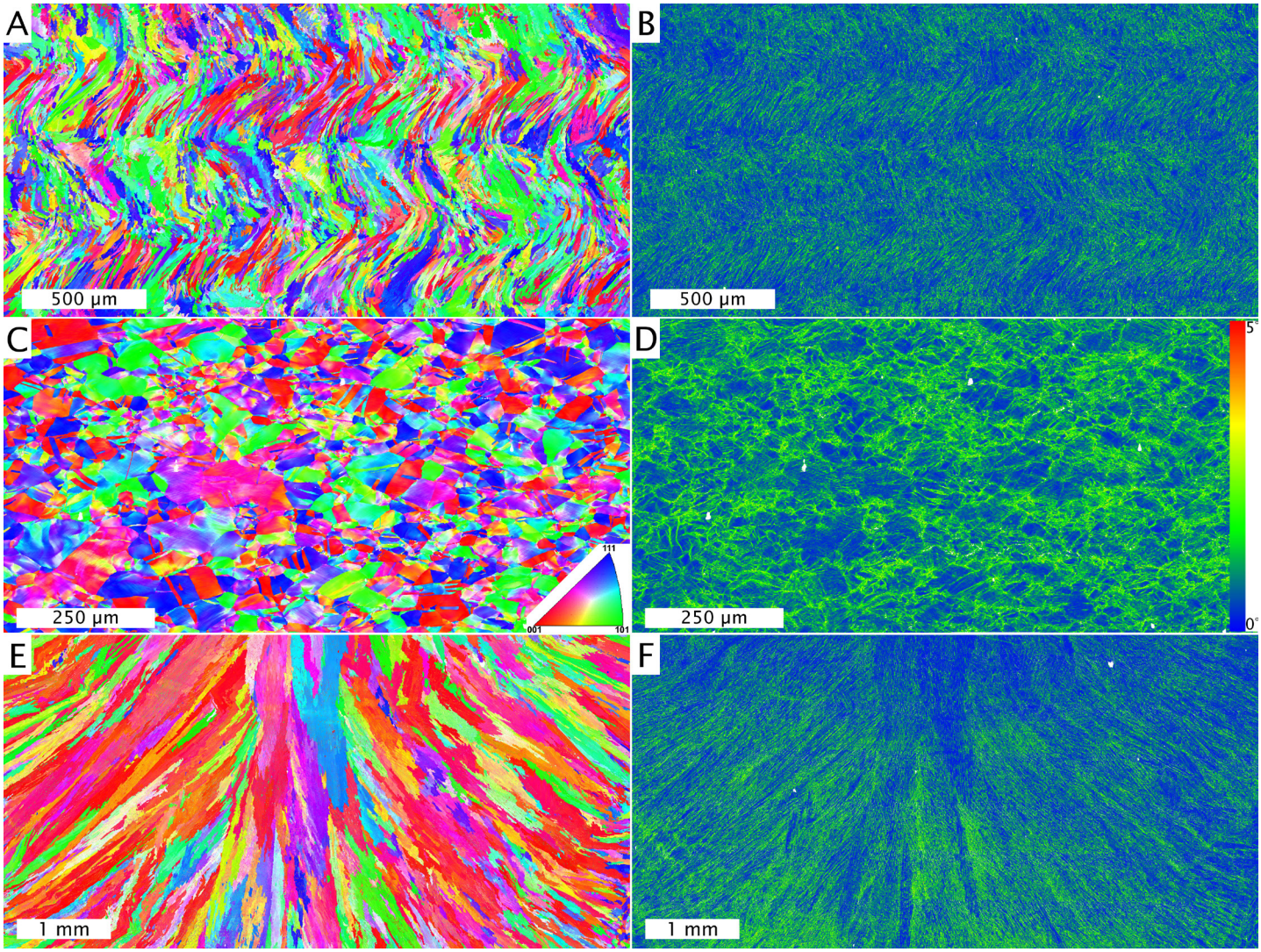

Figure 4. Electron backscattered diffraction (EBSD) inverse pole figure-z (IPF-z) orientation maps (OM) and kernel average misorientation (KAM) maps depicting the microstructures of A,B) DED 304L, C,D) forged 304L, and E,F) weld 308L/304L austenitic stainless steels.

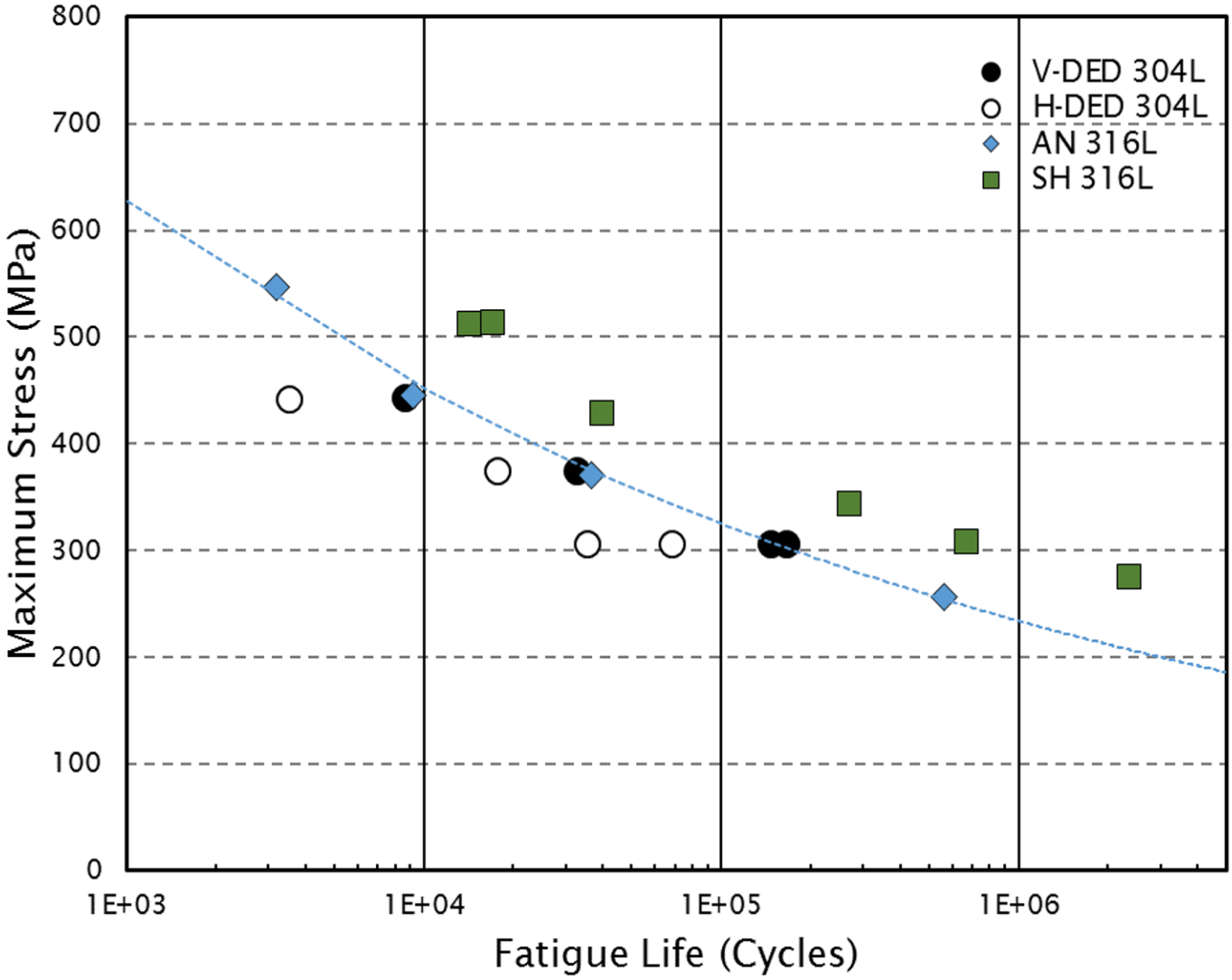

Figure 5. Fatigue life data for DED and wrought austenitic stainless steels. Fully dense material from the vertical DED (V-DED) build exhibited notched fatigue behavior commensurate with the strain hardened (SH) [20] and annealed (AN) [21] materials, while less dense material from the horizontal DED (H-DED) build possessed more variable fatigue properties.

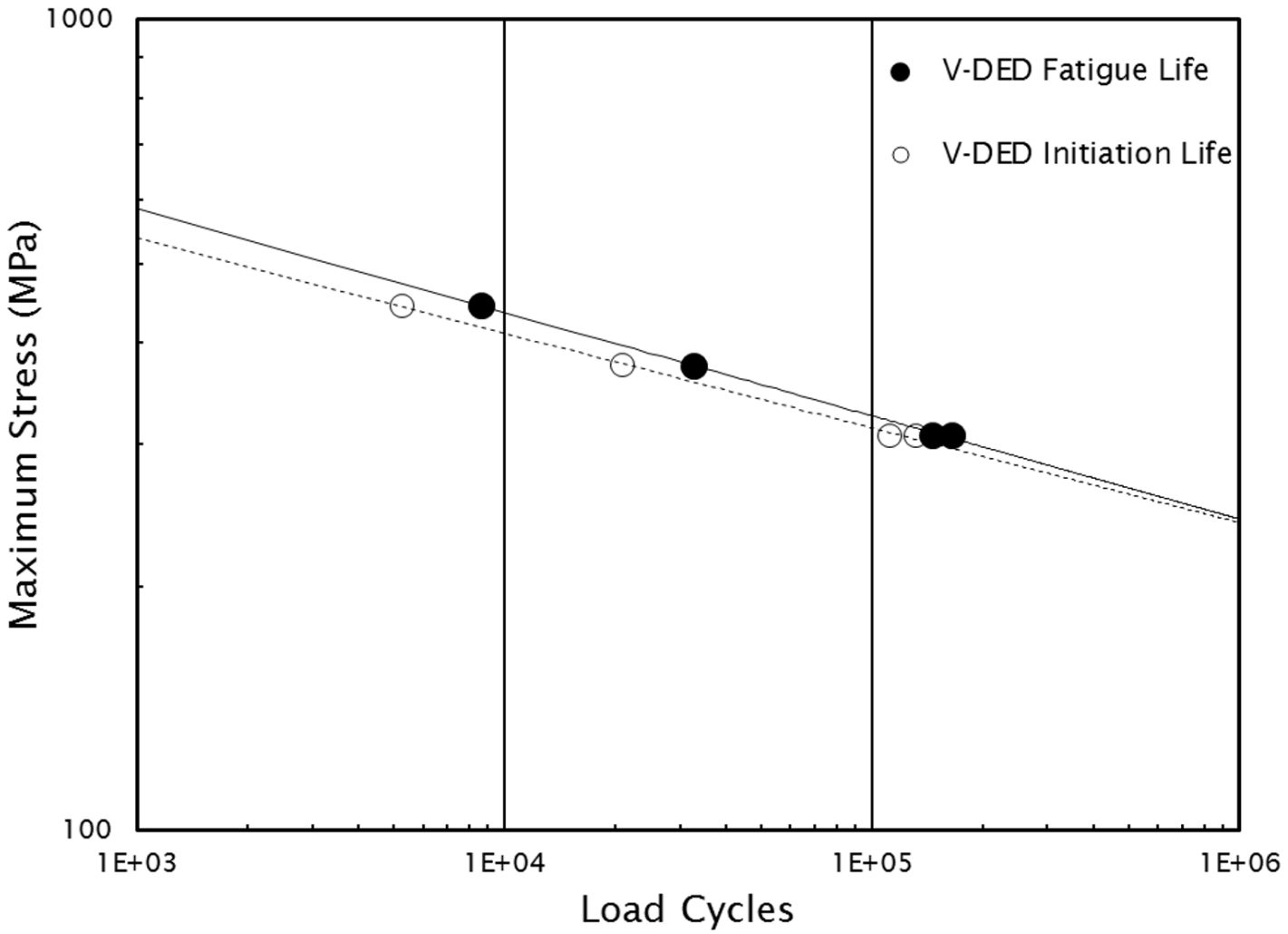

Figure 6. Comparison of fatigue life and fatigue crack initiation for V-DED determined by the direct current potential difference (DCPD) method.

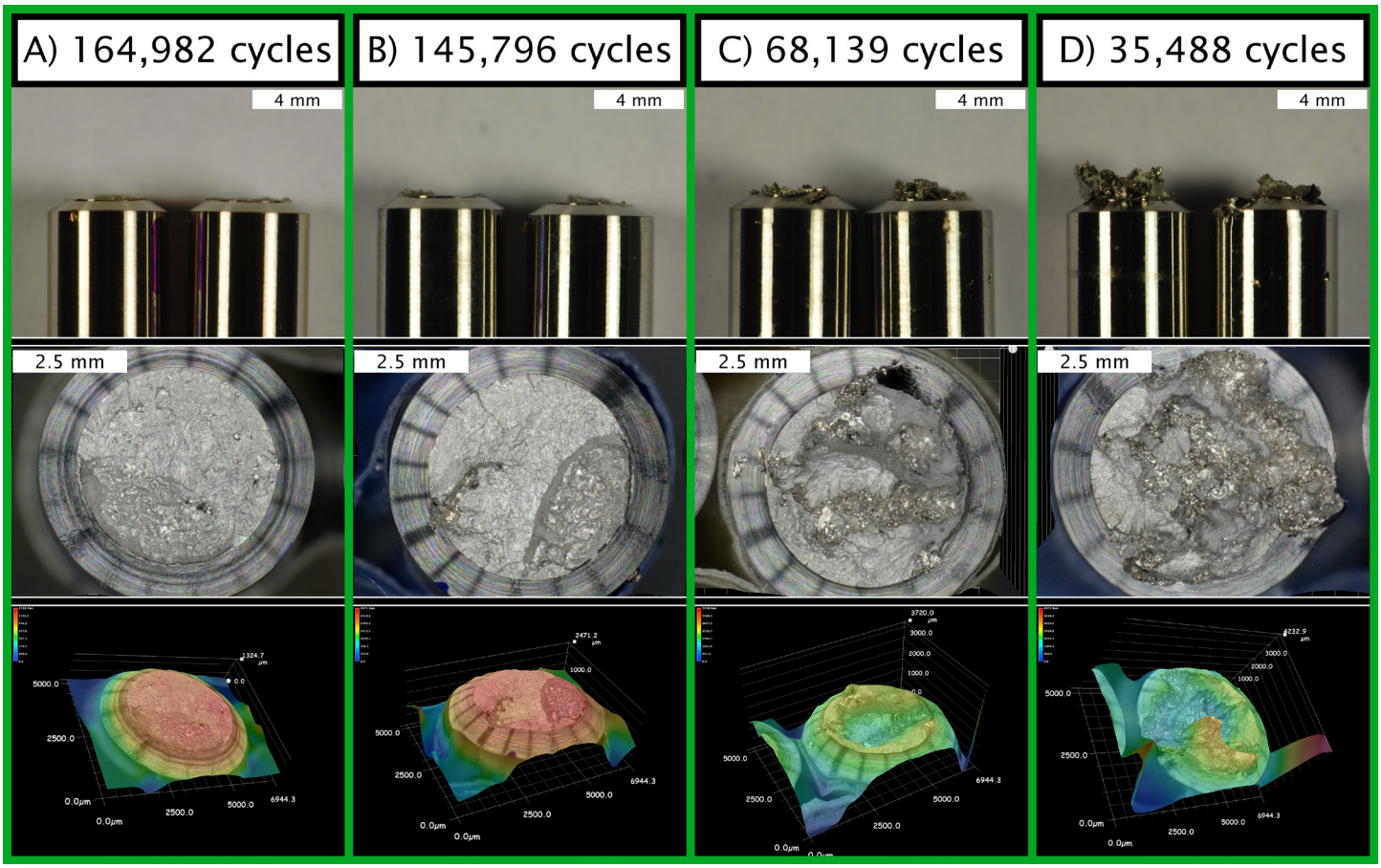

Figure 7. Photographs (top row), confocal micrographs (middle row), and confocal height maps (bottom row) depicting the variability in fracture surface morphology with number of cycles to failure for A,B) V-DED and C,D) H-DED fatigue specimens cycled at ~305 MPa maximum stress.